Research Square

Preprints are preliminary reports that have not undergone peer review. They should not be considered conclusive, used to inform clinical practice, or referenced by the media as validated information.

A new model for settling velocity of non-spherical particles

Fan Yang (erin_yangfan@whu.edu.cn)
Wuhan University School of Water Resources and Hydropower Engineering https://orcid.org/0000-0003-4306-4402

Yuhong Zeng
Wuhan University School of Water Resources and Hydropower Engineering

Wen-Xin Huai
Wuhan University School of Water Resources and Hydropower Engineering

Research Article

Keywords: Drag coefficient, Settling velocity, Sphericity, Non-spherical particles, Particle Reynolds number, shape-dependent functions

Posted Date: March 16th, 2021

DOI: https://doi.org/10.21203/rs.3.rs-269919/v1

License: This work is licensed under a Creative Commons Attribution 4.0 International License.
Read Full License

A new model for settling velocity of non-spherical particles

Fan Yang[1], Yu-Hong Zeng[1*], Wen-Xin Huai[1],

1. State Key Laboratory of Water Resources and Hydropower Engineering Science, Wuhan University, Wuhan, Hubei 430072, China

*Corresponding author (Y.H. Zeng)

Email: yhzeng@whu.edu.cn ;

Tel: +86 27 68772211;

Fax: +86 27 68772310.

ABSTRACT

The settlement of non-spherical particles, such as propagules of plants and natural sediments, are commonly observed in riverine ecosystems. The settling process is influenced by both particle properties (size, density and shape) and fluid properties (density and viscosity). Therefore, the drag law of non-spherical particles is a function of both particle Reynolds number and particle shape. Herein, a total of 828 settling data are collected from the literatures, which cover a wide range of particle Reynolds number (0.008-10000). To characterize the influence of particle shapes, sphericity is adopted as the general shape factor, which varies from 0.421 to 1.0. By comparing the measured drag with the standard drag curve of spheres, we modify the spherical drag law with three shape-dependent functions to develop a new drag law for non-spherical particles. Combined with an iterative procedure, a new model is thus obtained to predict the settling velocity of non-spherical particles of various shapes and materials. Further applications in hydrochorous propagule dispersal and sediment transport are projected based on deeper understanding of the settling process.

Keywords: Drag coefficient; Settling velocity; Sphericity; Non-spherical particles; Particle Reynolds number; shape-dependent functions.

1 Introduction

In riverine ecosystems, hydrochory plays a major role in transporting and depositing freshly-produced plants propagules (predominantly seeds) along the river corridors (Merritt & Wohl, 2002; Yoshikawa et al., 2013). In the way of becoming an essential part of the ecosystem, the non-buoyant seeds have to undergo a long period of settlement, dispersal, germination, and then gradually contribute to the colonization of the riparian zone (Gurnell et al., 2008; Chambert and James, 2009; Koch et al., 2010). Another factor that greatly affects the hydrodynamic process of rivers is the natural sediment. As mentioned by Meier et al. (2013), sediments can promote vegetation growth due to the transportation of nutrients and other organic matters. Moreover, by creating accretional structures in rivers, sediments can also facilitate the development of other species in the new habitats (Gurnell et al., 2012). Thus, as a starting point of the hydrodynamic process, the settlement of both hydrochorous seeds and natural sediments should be paid more attention since the construction of aquatic ecosystem grows more important.

Since all settlement issues are originated from the settlement of spheres, many spherical drag laws, whether explicit or implicit, are proposed by previous studies (Clift & Gauvin, 1971; Haider & Levenspiel, 1989; Brown & Lawler, 2003; Cheng, 2009; Terfous et al., 2013). However, in practical applications, the most commonly encountered particles (e.g., seeds, pebbles and gravels) are non-spherical and even irregular. Thus, the knowledge of drag coefficient and settling velocity of non-spherical particles is essential for solving the settling problem.

Based on numerous experimental and numerical settling data, many models have been proposed to predict the settling velocities of non-spherical particles. In these models, particles are usually separated into several categories, such as regular-shaped particles (Komar, 1980; Haider & Levenspiel, 1989; Ganser, 1993; Gogus et al., 2001; Wang et al., 2011; Lau & Chuah, 2013; Song et al., 2017), natural sediments and crushed rock fragments (Komar & Reimers, 1978; Hallermeier, 1981; Dietrich, 1982; Swamee & Ojha, 1991; Chien, 1994; Cheng, 1997; Alcerreca et al., 2013; Wang et al., 2017), and conglomerates of particles (Tran-Cong et al., 2004). Hence, the performances of most models are restricted in certain types of particles. Moreover, to scale the influence of non-spherical shapes of particles, different shape factors are applied. For instance, the factor, aspect ratio (E) is especially designed for the axisymmetric particles, such as cylinders, spheroids, and ellipsoids (Trans-Cong et al., 2004; Loth, 2008; Wang et al., 2011). The term S, which is defined as the ratio between equivalent sphere area and the projected area of particle settling direction, is also proposed to describe the effect of settling orientation (Song et al., 2017). Therefore, it is difficult to generalize the

effect of shape with one shape descriptor. Another problem for some models is that only part of the flow regimes is covered due to the limitation of experimental conditions. For instance, the model of Wang et al. (2017) is applicable for a certain range of particle Reynolds number, which varies from 0.01 to 3700. The range covers Strokes', intermediate, and early stage of Newton's flow regime. As for the settlement of particles in higher stage of Newton regime, the prediction ability of the model is unknown.

To solve the above-mentioned problems, a reliable model is developed based on a large amount of settling data, including irregular mineral sediments and artificial particles with non-spherical shapes. Note that behaviours of non-buoyant seeds during entrainment and settling are consistent with that of mineral sediments and the settling process of such artificial particles are analogous to that of natural sediments (Zhu et al., 2017). Herein, the shape factor, sphericity, is used as the general descriptor to show the influence of particle shapes. Note that the sphericity of these particles varies from 0.421 to 1.0. In addition, the particle Reynolds number ranges from 0.008 to 10000, which almost covers all regimes that can be encountered in natural processes. Herein, we modify the spherical drag law of Clift and Gauvin (1971) with shape-related functions to produce a new drag law for non-spherical particles. Subsequently, with an iterative procedure, a new model is developed to predict the settling velocity for different types of particles, which can eventually be applied in understanding the deposition, transport and dispersal of seeds and natural sediments.

1.1 In situ settling velocity

For particles settling through a static fluid, the balance between surface (drag) and body forces acting on the particle is expressed as follow:

$$\frac{1}{2}\rho_f C_d A_p W_s^2 = \left(\rho_s - \rho_f\right) gV \tag{1}$$

Therefore, the settling velocity of the particle can be obtained through the following formula:

$$W_s = \sqrt{\frac{4\left(\rho_s - \rho_f\right) g d_n}{3\rho_f C_d}} \tag{2}$$

where ρ_f is the fluid density, ρ_s is the particle density, C_d is the drag coefficient depending on properties of particle and fluid, A_p is the projected area of the particle perpendicular to the settling direction, W_s is the settling velocity of the particle, g is the gravitational acceleration, and V is the volume of the particle.

The particle Reynolds number (R_{ep}) is defined as:

$$\mathrm{R_{ep}} = \frac{\rho_f W_s d_n}{\mu} \tag{3}$$

where d_n is the diameter of the volume equivalent sphere, and μ is the dynamic viscosity of the fluid.

1.2 Particle shape characterization

For particles that are non-spherical, the diameter can be presented by the above-mentioned nominal diameter d_n to eliminate the influence of non-spherical shapes (Wadell, 1932).

$$d_n = \sqrt[3]{6V/\pi} \tag{4}$$

To describe the shape of non-spherical particles, multiple shape descriptors are proposed. For instance, the 1D descriptor, corey shape factor (*CSF*), is proposed by Corey (1963) to describe particles of relatively smooth surfaces. The term, circularity (*X*), is a 2D descriptor, which is suitable for particles with sharp corners and large obtuse angles (Büttner et al., 2002). However, since sphericity (ϕ) is the most widely used shape descriptor, and can accurately describe the shape of various particles, it is chosen in this study as the best descriptor. Sphericity is defined as the ratio between the surface area of the equivalent sphere A_{sph} and the particle surface area A_s:

$$\phi = \frac{A_{sph}}{A_s} \tag{5}$$

where A_{sph} is calculated by $A_{sph} = 4\pi\left(d_n/2\right)^2$.

For particles that are similar to scalene ellipsoids, the surface area of particle A_s can be approximately calculated as follow (Taylor et al., 2006):

$$A_s \approx 4\pi\left[\frac{(ab)^\lambda + (ac)^\lambda + (bc)^\lambda}{3 - k\left(1 - 27abc\left(a+b+c\right)^{-3}\right)}\right]^{1/\lambda} \tag{6}$$

where *a*, *b*, and *c* are semi-axes of a triaxial ellipsoid, λ =1.5349, k =0.0942.

Except for ϕ, another frequently used shape descriptor is ψ, which is defined as the ratio between sphericity and circularity ($\psi = \phi/X$). This descriptor is first introduced by Dellino et al. (2005) for highly irregular particles.

2 Materials and methods

2.1 Formulation

To develop a new shape-dependent drag law, we collect 828 sets of settling data from previous studies (Komar & Reimers, 1978; Komar, 1980; Baba & Komar, 1981; Chambert & James, 2009; Koch et al., 2010; Wang et al., 2011; Dioguardi & Mele, 2015; Song et al., 2017; Zhu et al., 2017). The new database mainly contains the settling data of volcanic materials and particles of regular shapes, such as cubes, cylinders, and cuboids. Details of the database are listed in Table 1. Note that within the database the range of ϕ is 0.421-1.0, and the value of R_{ep} varies from 0.008 to 10000.

Following the idea of Dioguardi et al. (2018), we construct a new drag law for non-spherical particles based on the spherical drag law of Clift and Gauvin (1971). This spherical drag law is chosen since it can effectively cover the entire R_{ep} range of the standard drag curve.

$$C_{d,sphere} = \frac{24}{\mathsf{R}_{ep}}\left(1+0.15\mathsf{R}_{ep}^{0.687}\right)+\frac{0.42}{1+\frac{42500}{\mathsf{R}_{ep}^{1.16}}} \tag{7}$$

By comparing the difference between the measured drag coefficient ($C_{d,meas}$) in our database and the drag of a sphere ($C_{d,sphere}$) at the same R_{ep}, we separate the Eq. (7) into the sum of three terms:

$$C_{d,sphere} = \frac{24}{\mathsf{R}_{ep}}+\frac{24}{\mathsf{R}_{ep}}\left(0.15\mathsf{R}_{ep}^{0.687}\right)+\frac{0.42}{1+\frac{42500}{\mathsf{R}_{ep}^{1.16}}} \tag{8}$$

In Fig. 1, we plot the measured drag coefficient of particles $C_{d,meas}$ versus the drag curve for spheres. The drag of non-spherical particles is observed to be larger than $C_{d,sphere}$ in most cases. Specifically, the measured drag (black dots) is close to $C_{d,sphere}$ (solid line) for R_{ep} <10. As R_{ep} grows larger than 10, the bias between the measured drag and the standard drag curve also becomes larger. In addition, for black dots that are closely related to the standard drag curve, the corresponding sphericities are close to 1.0. From these observations, we hypothesize that the influence of particle shape can be separately added to the three parts of Eq. (8).

$$C_{d,calc} = \frac{24}{\mathsf{R}_{ep}}f_1(\phi)+\frac{24}{\mathsf{R}_{ep}}\left(1+0.15\mathsf{R}_{ep}^{0.687}\right)f_2(\phi)+\frac{0.42}{1+\frac{42500}{\mathsf{R}_{ep}^{1.16}}}f_3(\phi) \tag{9}$$

For the shape-modified functions, the following constraints must be satisfied.

$$f_1(\phi=1)=f_2(\phi=1)=f_3(\phi=1)=1 \tag{10}$$

Therefore, when the shape of a particle is close to a sphere $(\phi \approx 1)$, Eq. (9) can turn back to the spherical drag law (Eq. (8)). Based on the collected database, the three functions are obtained by comparing the difference between $C_{d,meas}$ and $C_{d,sphere}$ focusing on the three parts separately. We also assume that the ratio between each terms of $C_{d,sphere}$ and the total $C_{d,sphere}$ is equal to the ratio between each part of $C_{d,meas}$ and the total drag of non-spherical particles (see Eq. (11)).

$$\frac{C_{d,sphere}(part)}{C_{d,sphere}(total)} = \frac{C_{d,meas}(part)}{C_{d,meas}(total)} \tag{11}$$

With this assumption, the three functions are separately searched by correlating each part of $C_{d,calc}$ with ϕ and R_{ep}. The best function is the one with the minimum error when predicting the settling velocity $W_{s,meas}$. Finally, the three functions satisfying the constraints and assumptions are:

$$f_1(\phi) = (2-\phi)^{\alpha_1} \tag{12a}$$

$$f_2(\phi) = \phi^{-\mathsf{R}_{\mathsf{ep}}^{\alpha_2}} \tag{12b}$$

$$f_3(\phi) = e^{\alpha_3(1-\phi)} \tag{12c}$$

The values of three exponents α_1, α_2, and α_3 are obtained by iteratively searching for the values that can present the best fit with the measured data. The iterative searching process is conducted with the Matlab script. The best values of α_1, α_2, and α_3 are 1.29, 0.134, and 1.43, respectively.

Thus, Eq. (9) turns to the new drag law:

$$C_{d,calc} = \frac{24}{\mathsf{R}_{\mathsf{ep}}}(2-\phi)^{1.29} + \frac{24}{\mathsf{R}_{\mathsf{ep}}}\left(1+0.15\mathsf{R}_{\mathsf{ep}}^{0.687}\right)\phi^{-\mathsf{R}_{\mathsf{ep}}^{0.134}} + \frac{0.42}{1+\dfrac{42500}{\mathsf{R}_{\mathsf{ep}}^{1.16}}}e^{1.43(1-\phi)} \tag{13}$$

As an implicit drag law depending on R_{ep}, an iterative procedure is usually adopted for calculating C_d, since both C_d and R_{ep} are relevant to W_s. The trial-and-error procedure is presented in the flow chart (Fig. 2). Details of the new drag law can be found in the Online Resource (sheet of "Drag law").

2.2 *Models for comparison*

To evaluate the ability of the present model to predict the settling velocity of non-spherical particles, we compare it with previous models (Chien, 1994; Alcerreca et al., 2013; Dioguardi & Mele, 2015; Dioguardi et al., 2018). Details of comparison with other models are given in the Online Resource (sheet of "Model comparison").

Chien (1994) derived the drag law for irregular particles settling in Newtonian and non-Newtonian fluids. Since this drag law is also implicit, a numerical iteration method is required to predict the settling velocity. The model of Chien (1994) covers a ϕ range of 0.2-1.0, and a $\mathrm{R_{ep}}$ range of 0.001-10000.

$$C_d = \frac{30}{\mathrm{R_{ep}}} + \frac{67.289}{e^{5.03\phi}} \tag{14}$$

The drag law of Alcerreca et al. (2013) is derived based on a large amount of settling data of calcareous sand particles. The drag law is explicit since C_d can be expressed as a function of the dimensionless particle diameter $\mathrm{D_*}$:

$$C_d = \frac{4}{3}\frac{\mathrm{D_*^3}}{\mathrm{R_{ep}}^2} \tag{15a}$$

$$\mathrm{R_{ep}} = \frac{\rho_f W_s d_n}{\mu} = \left(\sqrt{22 + 1.13\mathrm{D_*^2}} - 4.67\right)^{1.5} \tag{15b}$$

$$\mathrm{D_*} = d_N\left[\left(g/\upsilon^2\right)\left(\rho_s/\rho_f - 1\right)\right]^{1/3} \tag{15c}$$

where d_N is the nominal particle diameter which can be calculated by $d_N = \left(d_l d_m d_s\right)^{1/3}$, and υ is the kinematic viscosity of the fluid. Note that d_l, d_m, d_s means the lengths of the longest, intermediate, and shortest principle axes of the particle, respectively. Consequently, the settling velocity can be calculated directly from basic properties of particles and fluids ($d_l, d_m, d_s, \rho_s, \rho_f, \upsilon$).

Dioguardi and Mele (2015) applied the shape factor ψ to describe the irregularity of particles. Their drag law is based on the 340 settling data of volcanic particles, which are in a wide range of $\mathrm{R_{ep}}$ (0.03-10000). Developed from the drag law of Dellino et al. (2005), the form of this law is segmented and simple:

$$C_d = \frac{C_{d,sphere}}{\mathrm{R_{ep}}^2 \psi^{\exp}}\left(\frac{\mathrm{R_{ep}}}{1.1883}\right)^{\frac{1}{0.4826}} \tag{16}$$

$$\exp = \mathrm{R_{ep}}^{-0.23} \text{ for the Re ranges of 0-50;}$$

$$\exp = \mathrm{R_{ep}}^{0.05} \text{ for the Re ranges of 50-10000;}$$

where $C_{d,sphere}$ is calculated by the drag law of Clift and Gauvin (1971) (see Eq. (7)). An iterative procedure is needed to construct the final model to predict the terminal settling velocity.

As a development of Dioguardi and Mele (2015), the model of Dioguardi et al. (2018) also used the shape factor ψ. Their drag law is obtained by 304 settling velocity measurements,

which are part of the 340 settling data mentioned in Table 1. Note that the structure of this model is similar to the present model (Eq. (13)). Differences between the two models are discussed in Section 3.

$$C_{d,calc} = \frac{24}{\mathsf{R}_{\mathsf{ep}}}\left(\frac{1-\psi}{\mathsf{R}_{\mathsf{ep}}}+1\right)^{0.25} + \frac{24}{\mathsf{R}_{\mathsf{ep}}}\left(0.1806\mathsf{R}_{\mathsf{ep}}^{\ 0.6459}\right)\psi^{-\left(\mathsf{R}_{\mathsf{ep}}^{\ 0.08}\right)} + \frac{0.4251}{1+\dfrac{6880.95}{\mathsf{R}_{\mathsf{ep}}}\psi^{5.05}} \tag{17}$$

2.3 Comparison results

To compare the accuracy of predicting the settling velocity for each model, we first plot the $C_{d,calc}$ and $C_{d,meas}$ versus R_{ep} in Fig. 3. After calculating the $C_{d,calc}$ with the aforementioned laws, we iteratively obtain the terminal settling velocity $W_{s,calc}$ and compare it with the measured values $W_{s,meas}$. In Fig. 4, the comparison results are displayed, along with the correlation coefficient of each model. As shown in Fig. 4, most models have similar correlation coefficients, which are approximately 0.94. The performance of Alcerecca et al. (2013) is relatively weak, which may due to the fact that their model is based on settling data of calcareous sand. Thus, for non-spherical particles of other shapes and materials, the ability of this model to predict the settling velocity is limited.

Based on the correlations between $W_{s,calc}$ and $W_{s,meas}$, three statistical parameters are used as indicators to assess the ability of different models to predict the settling velocity of non-spherical particles. The first parameter is the R-squared (R^2), which is obtained by linear fitting and presented in Fig. 4 for each model. The second parameter is average absolute error (|err%|), which is calculated as follow:

$$|err\%| = \frac{\left|W_{s,calc} - W_{s,meas}\right|}{W_{s,meas}} \times 100 \tag{18}$$

We also evaluate each model with the root-mean-square error (RMSE) by applying the following formula:

$$RMSE = \sqrt{\frac{\sum_{i=1}^{N}\left(\dfrac{W_{s,calc,i} - W_{s,meas,i}}{W_{s,meas,i}}\right)^2}{N}} \times 100 \tag{19}$$

where N=828 is the number of settling data in our database.

Error analyses of the three indicators for different models are summarized in Table 2. From R^2 listed in Table 2, the performance of the present model is slightly weaker than the model of Dioguardi et al. (2018). However, when evaluating the performance of models by |err%| and RMSE, the present model predicts the settling velocity better than all the other models.

To further explore the differences among these models, we compare the ability of each model to predict settling velocity of particles from different sources. The comparisons of |err%| are given in Table 3 while the results of RMSE are summarized in Table 4. About the two tables, two notations are clarified. Firstly, since the number of settling data of hydrochorous seeds is low, we summarize the settling data of seeds from three sources in one row, which is simply marked as "Hydrochorous seeds" (Chambert & James, 2009; Koch et al., 2010; Zhu et al., 2017). Secondly, since the data of tri-axial lengths are missing for hydrochorous seeds, the shape descriptor ψ mentioned in the models of Dioguardi and Mele (2015) and Dioguardi et al. (2018) cannot be calculated. Thus, in the last row of both tables, the error analyses for hydrochorous seeds are not given for the two models.

From Table 3 and 4, the present model performs quite well for data collected from Song et al. (2017), Komar and Reimers (1978) and Baba and Komar (1981). Combined with particle shapes and materials listed in Table 1, the present model is found to be especially suitable for regular particles (e.g., cubes and cylinders) and particles with relatively smooth surfaces (e.g., pebbles and irregular glass particles). Nevertheless, the accuracy of the present model to predict the settling velocities for data from Wang et al. (2011), Komar (1980) and Hydrochorous seeds is only acceptable. For data from Wang et al. (2011), Komar (1980), the present model performs better than the other models except for the model of Dioguardi and Mele (2015). The prediction for settling velocity of Hydrochorous seeds, though not accurate enough, is the best among these models. A common reason for the deviations is that all the settling data from the three sources are no more than 50 data points, and thus the errors may be enlarged. At last, the abilities of the models to predict settling velocity of volcanic particles are compared. Since the models of both Dioguardi and Mele (2015) and Dioguardi et al. (2018) are developed from the settling data of volcanic materials, they naturally show smaller errors than the other models. Note that the performance of the present model is just slightly weaker than the two models. To summarize from the above analysis, it can be concluded that the present model shows the best performance when predicting settling velocity for particles of various shapes and materials.

3 Discussion

Among these models for comparison, the differences between the model of Dioguardi et al. (2018) and the present model need to be further discussed, since they are based on similar ideas. Herein, four major differeces are clarified. Firstly, as shown in Table 1, the present model contains a larger database, which includes particles of various shapes and materials. On the other hand, the model of Dioguardi et al. (2018) is based on only part of the 340 data points of volcanic particles. Secondly, the shape factor applied by Dioguardi et al. (2018) is

ψ rather than ϕ. As mentioned in Section 1.2, the calculation of ψ requires the value of circularity (X) in addition to sphericity (ϕ). Thus, the model of Dioguardi et al. (2018) has more difficulty in application. Thirdly, the first and last shape-modified functions of the present model ($f_1(\phi)$ and $f_3(\phi)$ in Eq. (13)) have different forms and positions with that of the model of Dioguardi et al. (2018) (Eq. (17)). Lastly, the model of Dioguardi et al. (2018) is based on the spherical drag law of Haider and Levenspiel (1989), which is suitable for $\mathsf{R}_{ep} < 2.6\times10^5$.

Developed from the idea of Dioguardi et al. (2018), the present model enhances the applicability in predicting the terminal settling velocity for particles of various shapes and materials, and thus can be considered as an improvement.

4 Conclusion

We propose a new drag law for non-spherical particles based on a total of 828 settling data collected from previous studies (Komar & Reimers, 1978; Komar, 1980; Baba & Komar, 1981; Chambert & James, 2009; Koch et al., 2010; Wang et al., 2011; Dioguardi & Mele, 2015; Song et al., 2017; Zhu et al., 2017). This new database cover a R_{ep} range of 0.008~10000 and a ϕ range of 0.421~1.0. Thus, the new model is suitable for the settlement of non-spherical particles in both laminar and turbulent flows. In addition, since this new model is developed from settling data from various sources, it can be applied in predicting settling velocity of regular particles (e.g., cubes, cylinders, and cuboids), natural particles (e.g., volcanic particles, pebbles, and glass particles of various shapes), and even non-spherical hydrochorous seeds.

Following the idea of Dioguardi et al. (2018), the new model adopts three shaped-modified functions in the spherical drag law of Clift and Gauvin (1971). With these functions based on R_{ep} and ϕ, the new model exhibits better performance than the other models. With the wide range of applicability in both flow regimes and particle shapes, the present model may be practical in solving problems concerning the riverine ecosystem. On the one hand, by relating the settling process of seeds with the dispersal process, more detailed information can be obtained about the germination of seeds and establishment of aquatic vegetation, which is crucial for flow characteristics in river systems (Meier et al., 2013). On the other hand, the advanced settling model can estimate the rate of sediment transport for various particles and flow regimes by being applied in predicting the distribution of sediment concentration (Fu et al., 2005; Graf and Cellino, 2002). Such application may be verified when provided with further sediment concentration profile measurements of irregular particles. In addition to its

application in the riverine ecosystems, the new settling model may be further improved by extending from the drag of single irregular particle to conglomerates of particles.

Declarations

Ethical approval and consent to participate

Not applicable

Consent for publication

Not applicable

Availability of data and materials

All data generated or analysed during this study are included in the supplementary information files, which can be found in the online version of this article.

Competing interests

The authors declare that they have no competing interests

Funding

This work is financially supported by the National Natural Science Foundation of China (Nos. 51879197, 51622905).

Authors' contributions

All authors contributed to the model conception and derivation. F. Yang: data curation, methodology, formal analysis, writing - original draft; Y.H. Zeng: conceptualization, funding acquisition, supervision, writing - review & editing; W.X. Huai: conceptualization, writing - review & editing. All authors have read and approved the final manuscript.

Notation

a, b, c	= Semi-axes of a tri-axial ellipsoid (m)
A_p	= Projected area perpendicular to the flow direction (m^2)
A_s	= Total surface area of the particle (m^2)
A_{sph}	= Surface area of equivalent spheres (m^2)

C_d	= Drag coefficient (-)
$C_{d,calc}$	= Calculated drag coefficient (-)
$C_{d,meas}$	= Measured drag coefficient (-)
$C_{d,sphere}$	= Drag coefficient of sphere (-)
d_n	= Diameter of the volume equivalent sphere (m)
d_N	= Nominal particle diameter (m)
d_l, d_m, d_s	= Lengths of the longest, intermediate, and shortest principle axes of the particle (m)
D_*	= Dimensionless particle diameter (-)
E	= Aspect ratio (-)
g	= Gravitational acceleration (m s^{-2})
R_{ep}	= Particle Reynolds number (-)
S	= The ratio between equivalent sphere area and the projected area of particle settling direction (-)
V	= Volume of the particle (m^3)
W_s	= Settling velocity of particles (m s^{-1})
$W_{s,calc}$	= Calculated settling velocity of particles (m s^{-1})
$W_{s,meas}$	= Measured settling velocity of particles (m s^{-1})
X	= Particle circularity (-)
ρ_s	= Particle density (kg m^{-3})
ρ_f	= Fluid density (kg m^{-3})
μ	= Dynamic viscosity (kg m^{-1} s^{-1})
υ	= Kinematic viscosity (m^2 s^{-1})
ϕ	= Particle sphericity (-)
ψ	= Shape descriptor (-)
λ, k	= Parameters in Eq. (6) (-)
$\alpha_1, \alpha_2, \alpha_3$	= Exponents in Eq. (12) (a, b, c) (-)

References

Alcerreca, J., Silva, R., & Mendoza, E. (2013). Simple settling velocity formula for calcareous sand. *Journal of Hydraulic Research*, 51, 215-219. http://dx.doi.org/10.1080/00221686.2012.753645

Baba, J., & Komar, P. D. (1981). Settling velocities of irregular grains at low Reynolds numbers. *Journal of Sedimentary Petrology*, 51, 121-128. http://dx.doi.org/10.1306/212F7C25-2B24-11D7-8648000102C1865D

Brown, P. P., & Lawler, D. F. (2003). Sphere drag and settling velocity revisited. *Journal of Environmental Engineering*, 123, 222-231. http://dx.doi.org/10.1061/(ASCE)0733-9372(2003)129:3(222)

Büttner, R., Dellino, P., La Volpe, L., Lorenz, V., & Zimanowski, B. (2002). Thermohydraulic explosions in phreatomagmatic eruptions as evidenced by the comparison between pyroclasts and products from molten fuel coolant interactions experiments. *Journal of Geophysical Research-Solid Earth*, 107. http://dx.doi.org/10.1029/2001JB000511

Chambert, S., & James, C. S. (2009). Sorting of seeds by hydrochory. *River Research and Applications*, 25, 48-61. http://dx.doi.org/10.1002/rra.1093

Cheng, N. S. (1997). Simplified settling velocity formula for sediment particle. *Journal of Hydraulic Engineering*, 123, 149-152. http://dx.doi.org/10.1061/(ASCE)0733-9429(1997)123:2(149)

Cheng, N. S. (2009). Comparison of formulas for drag coefficient and settling velocity of spherical particles. *Powder Technology*, 189, 395-398. http://dx.doi.org/10.1016/j.powtec.2008.07.006

Chien, S. F. (1994). Settling velocity of irregularly shaped particles. *SPE Drilling & Competition*, 9, 281-289. http://dx.doi.org/10.2118/26121-PA

Clift, R., & Gauvin, W. H. (1971). Motion of entrained particles in gas streams. *Canadian Journal of Chemical Engineering*, 49, 439-448. http://dx.doi.org/10.1002/cjce.5450490403.

Corey, A. T. (1963). *Influence of shape on the fall velocity of sand grains.* Colorado State University Audio Visual Service.

Dellino, P., Mele, D., Bonasia, R., Braia, G., La Volpe, L., & Sulpizio, R. (2005). The analysis of the influence of pumice shape on its terminal velocity. *Geophysical Research Letters*, 32. http://dx.doi.org/10.1029/2005GL023954

Dietrich, W. E. (1982). Settling velocity of natural particles. *Water Resources Research*, 18, 1615-1626. http://dx.doi.org/10.1029/WR018i006p01615

Dioguardi, F., Mele, D., & Dellino, P. (2018). A new one-equation model of fluid drag for irregularly shaped particles valid over a wide range of Reynolds number. *Journal of Geophysical Research: Solid Earth*, 123, 144-156. http://dx.doi.org/10.1002/2017JB014926

Dioguardi, F., & Mele, D. (2015). A new shape dependent drag correlation formula for non-spherical rough particles. Experiments and results. *Powder Technology*, 277, 222-230. http://dx.doi.org/10.1016/j.powtec.2015.02.062

Fu, X., Wang, G., & Shao, X. (2005). Vertical dispersion of fine and coarse sediments in turbulent open-channel flows. *Journal of Hydraulic Engineering*, 131, 877-888. https://doi.org/10.1061/(ASCE)0733-9429(2005) 131:10(877)

Ganser, G. H. (1993). A rational approach to drag prediction of spherical and non-spherical particles. *Powder Technology*, 77, 143-152. http://dx.doi.org/10.1016/0032-5910(93)80051-B

Gogus, M., Ipekci, O. N., & Kokpinar, M. A. (2001). Effect of particle shape on fall velocity of angular particles. *Journal of Hydraulic Engineering*, 127, 860-869. http://dx.doi.org/10.1061/(ASCE)0733-9429(2001)127:10(860)

Graf, W. H., & Cellino, M. (2002). Suspension flows in open channels: experiment study. *Journal of Hydraulic Research*, 40, 435-447. https://doi.org/10.1080/00221680209499886.

Gurnell, A. M., Thompson, K., Goodson, J., & Moggridge, H. (2008). Propagule deposition along river margins: linking hydrology and ecology. *Journal of Ecology*, 96, 553-565. http://dx.doi.org/10.1111/j.1365-2745.2008.01358.x

Gurnell, A. M., Bertoldi, W., & Corenblit, D. (2012). Changing river channels: The roles of hydrological processes, plants and pioneer fluvial landforms in humid temperature, mixed load, gravel bed rivers. *Earth-Science Reviews*, 111, 129-141. http://dx.doi.org/10.1016/j.earscirev.2011.11.005

Haider, A., & Levenspiel, O. (1989). Drag coefficient and terminal velocity of spherical and non-spherical particles. *Powder Technology*, 58, 63-70. http://dx.doi.org/10.1016/0032-5910(89)80008-7

Hallermeier, R. (1981). Terminal settling velocity of commonly occurring sand grains. *Sedimentology*, 28, 859-865. http://dx.doi.org/10.1111/j.1365-3091.1981.tb01948.x

Koch, E. W., Ailstock, M. S., Booth, D. M., Shafer, D. J., & Magoun, A. D. (2010). The role of currents and waves in the dispersal of submersed angiosperm seeds and seedlings. *Restoration Ecology*, 18, 584-595. http://dx.doi.org/10.1111/j.1526-100X.2010.00698.x

Komar, P. D., & Reimers, C.E. (1978). Grain shape effects on settling rates. *Journal of Geology*, 86, 193-209. http://dx.doi.org/10.1086/649674

Komar, P. D. (1980). Settling velocities of circular cylinders at low Reynolds numbers. *Journal of Geology*, 88, 327-336. http://dx.doi.org/10.1086/628510

Lau, R., & Chuah, H. (2013). Dynamic shape factor for particles of various shapes in the intermediate settling regime. *Advanced Powder Technology*, 24, 306-310. http://dx.doi.org/10.1016/j.apt.2012.08.001

Loth, E. (2008). Drag of non-spherical solid particles of regular and irregular shape. *Powder Technology*, 182, 342-353. http://dx.doi.org/10.1016/j.powtec.2007.06.001

Merritt, D. M., & Wohl, E. E. (2002). Processes governing hydrochory along rivers:

hydraulics, hydrology, and dispersal phenology. *Ecological Applications*, 12, 1071-1087. http://dx.doi.org/10.1890/1051-0761(2002)012[1071:PGHARH]2.0.CO;2

Meier, C. I., Reid, B. L., & Sandoval, O. (2013). Effects of the invasive plant Lupinus polyphyllus on vertical accretion of fine sediment and nutrient availability in bars of the gravel-bed Paloma river. *Limnologica-Ecology and Management of Inland Waters*, 43, 381–387. http://dx.doi.org/10.1016/j.limno.2013.05.004

Song, X. Z., Xu, Z. M., Li, G. S., Pang, Z. Y., & Zhu, Z. P. (2017). A new model for predicting drag coefficient and settling velocity of spherical and non-spherical particle in Newtonian fluid. *Powder Technology*, 321, 242-250. http://dx.doi.org/10.1016/j.powtec.2017.08.017

Swamee, P., & Ojha, C. (1991). Drag coefficient and fall velocity of non-spherical particles. *Journal of Hydraulic Engineering.*, 117, 660-667. http://dx.doi.org/10.1061/(ASCE)0733-9429(1991)117:5(660)

Taylor, M. A., Garboczi, E. J., Erdogan, S. T., & Fowler, D. W. (2006). Some properties of irregular 3-D particles. *Powder Technology*, 162, 1-15. http://dx.doi.org/10.1016/j.powtec.2005.10.013

Terfous, A., Hazzab, A., & Ghenaim, A. (2013). Predicting the drag coefficient and settling velocity of spherical particles. *Powder Technology*, 239, 12-20. http://dx.doi.org/10.1016/j.powtec.2013.01.052

Tran-Cong, S., Gay, M., & Michaelides, E. E. (2004). Drag coefficients of irregularly shaped particles. *Powder Technology*, 139, 21-32. http://dx.doi.org/10.1016/j.powtec.2003.10.002

Wadell, H. (1932). Volume, shape, and roundness of rock particles. *Journal of Geology*, 40, 443-451. http://dx.doi.org/10.1086/623964.

Wang, J. S., Qi, H. Y., & Zhu, J. Z. (2011). Experimental study of settling and drag on cuboids with square base. *Particuology*, 9, 298-305. http://dx.doi.org/10.1016/j.partic.2010.11.002

Wang, Y., Zhou, L. X., Wu, Y., & Yang, Q. (2017). New simple correlation formula for the drag coefficient of calcareous sand particles of highly irregular shape. *Powder Technology*, 326, 379-392. http://dx.doi.org/10.1016/j.powtec.2017.12.004

Yoshikawa, M., Hoshino, Y., & Iwata, N. (2013). Role of seed settleability and settling velocity in water for plant colonization of river gravel bars. *Journal of Vegetation Science*, 24, 712-723. http://dx.doi.org/10.1111/jvs.12001

Zhu, X., Zeng, Y. H., & Huai, W. X. (2017). Settling velocity of non-spherical hydrochorous seeds. *Advances in Water Resources*, 103, 99-107. http://dx.doi.org/10.1016/j.advwatres.2017.03.001

List of tables

Table 1 Sources of data

Source	Number of points	Particle types
Song et al. (2017)	276	Cube, cylinder
Dioguardi and Mele (2015)	340	Volcanic materials
Wang et al. (2011)	48	Cuboids
Komar and Reimers (1978)	51	Ellipsoidal pebbles
Baba and Komar (1981)	72	Irregular glass particles
Komar (1980)	27	Cylindrical-shaped grains
Chambert and James (2009)	8	Non-spherical seeds
Koch et al. (2010)	3	Non-spherical seeds
Zhu et al. (2017)	3	Non-spherical seeds

Table 2 Performance comparison of models

Model	R^2	|err%|	RMSE
Chien (1994)	0.930	13.347	18.664
Alcerreca et al. (2013)	0.904	18.270	28.098
Dioguardi and Mele (2015)	0.941*	16.186*	20.142*
Dioguardi et al. (2018)	0.951*	11.652*	15.800*
Present model	0.943	9.624	15.061

Note: Data marked with asterisk are obtained without considering the settlement of hydrochorous seeds. The data are still convincible since the settling data of seeds (14 data points) only account for 1.69% of the total database (828 data points).

Table 3 Comparisons of models by |err%|

Data source	Chien (1994)	Alcerecca et al. (2013)	Dioguardi and Mele (2015)	Dioguardi et al. (2018)	Present model
Song et al. (2017)	22.790	13.507	17.314	12.23	7.234
Dioguardi and Mele (2015)	15.233	14.701	11.123	10.69	11.587
Wang et al. (2011)	16.747	15.646	20.800	16.25	17.627
Komar and Reimers (1978)	8.407	4.847	24.692	7.35	2.590
Baba and Komar (1981)	9.733	3.418	25.356	10.30	3.790
Komar (1980)	54.307	27.107	19.701	21.394	20.435
Hydrochorous seeds	18.455	24.914	/	/	16.424

Table 4 Comparisons of models by RMSE

Data source	Chien (1994)	Alcerecca et al. (2013)	Dioguardi and Mele (2015)	Dioguardi et al. (2018)	Present model
Song et al. (2017)	36.102	18.560	21.313	17.143	13.058
Dioguardi and Mele (2015)	19.240	19.040	13.777	14.362	16.465
Wang et al. (2011)	21.374	22.618	27.009	19.958	21.339
Komar and Reimers (1978)	10.406	6.100	25.512	8.980	3.165
Baba and Komar (1981)	11.173	4.268	27.401	11.693	4.863
Komar (1980)	68.173	32.323	25.876	26.451	26.529
Hydrochorous seeds	21.001	31.771	/	/	19.830

Figures

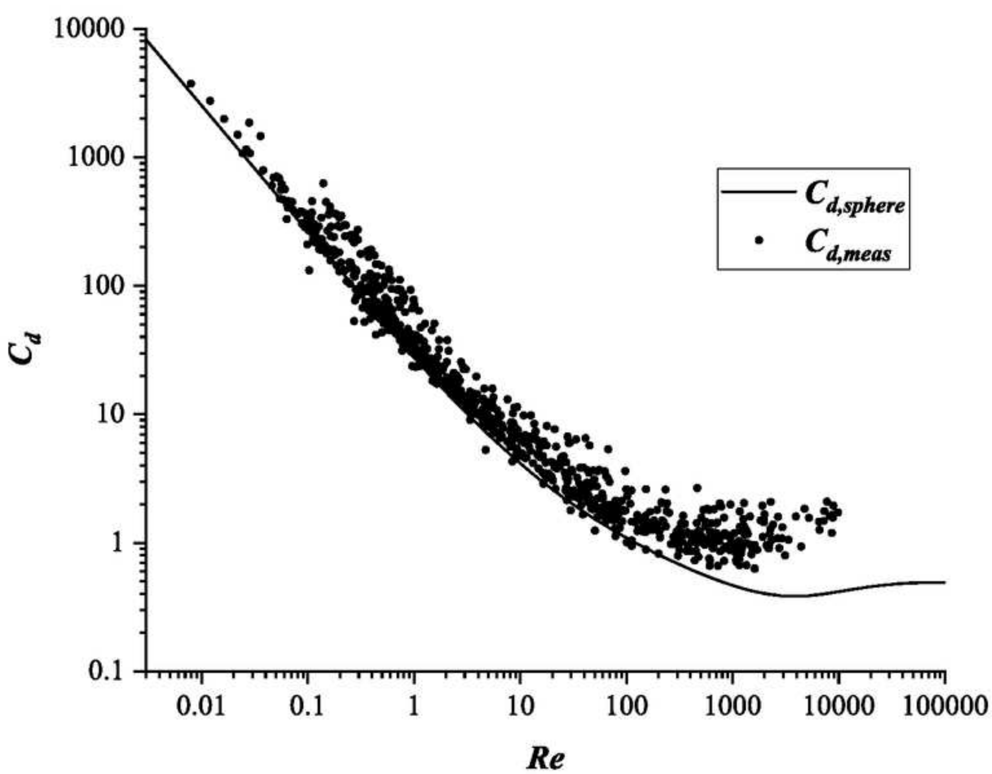

Figure 1

See manuscript for full figure caption.

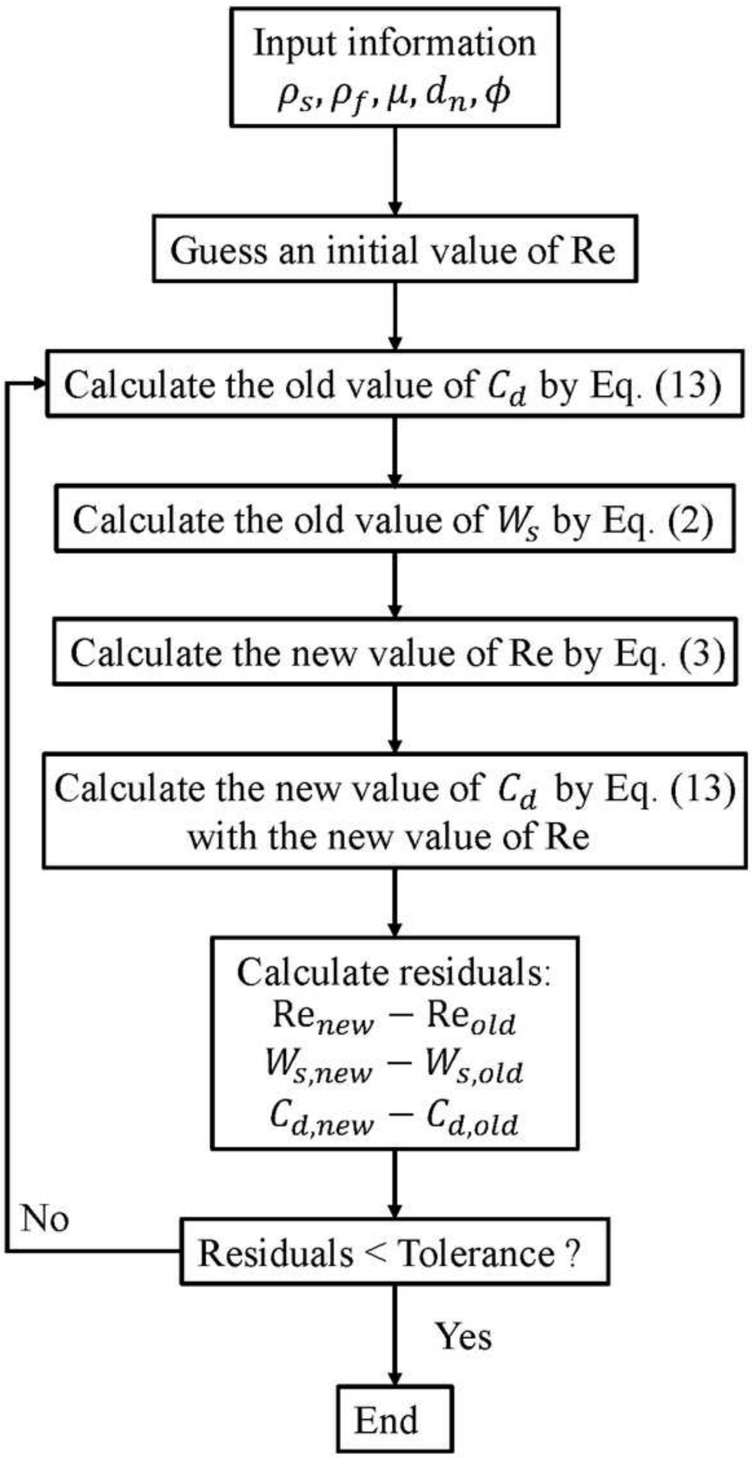

Figure 2

The trial-and-error procedure is presented in the flow chart

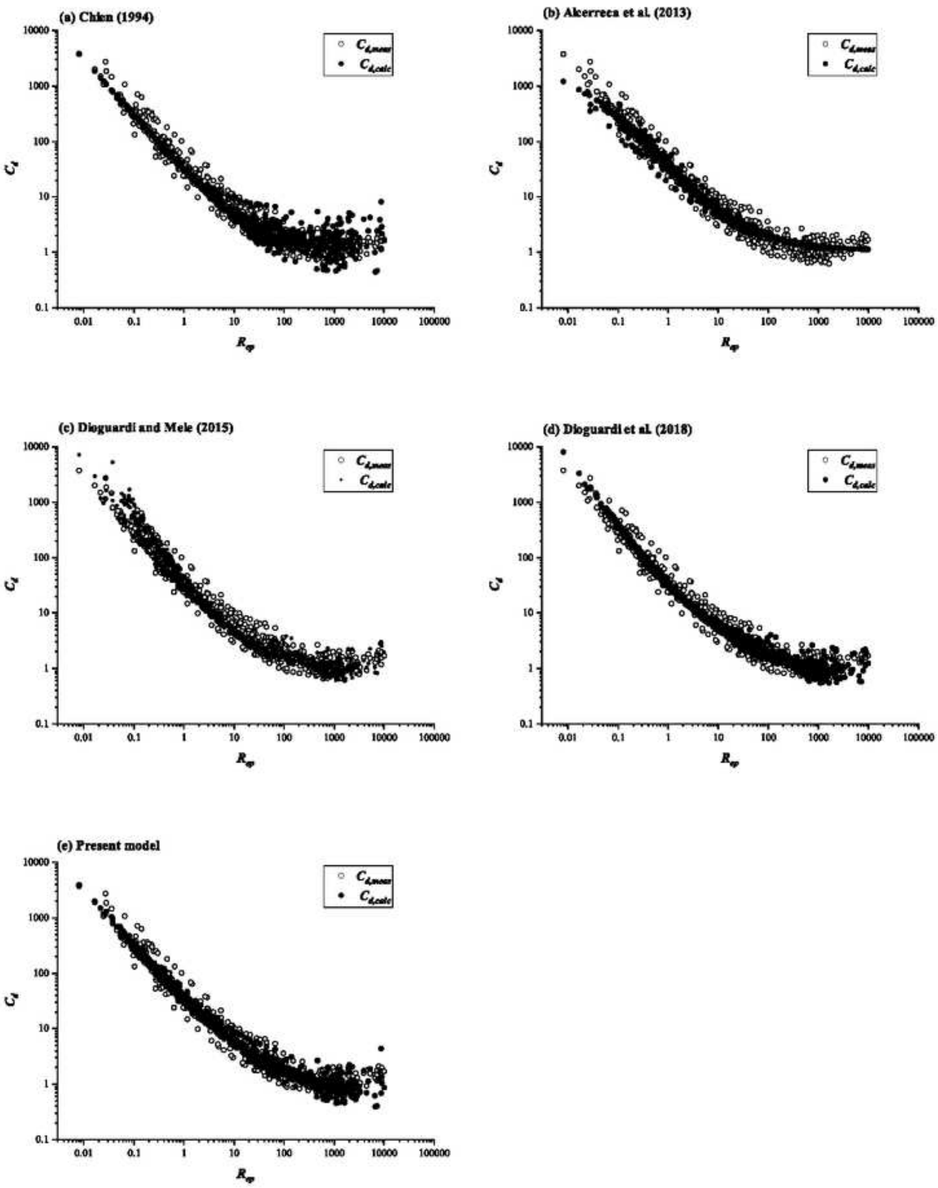

Figure 3

See manuscript for full figure caption.

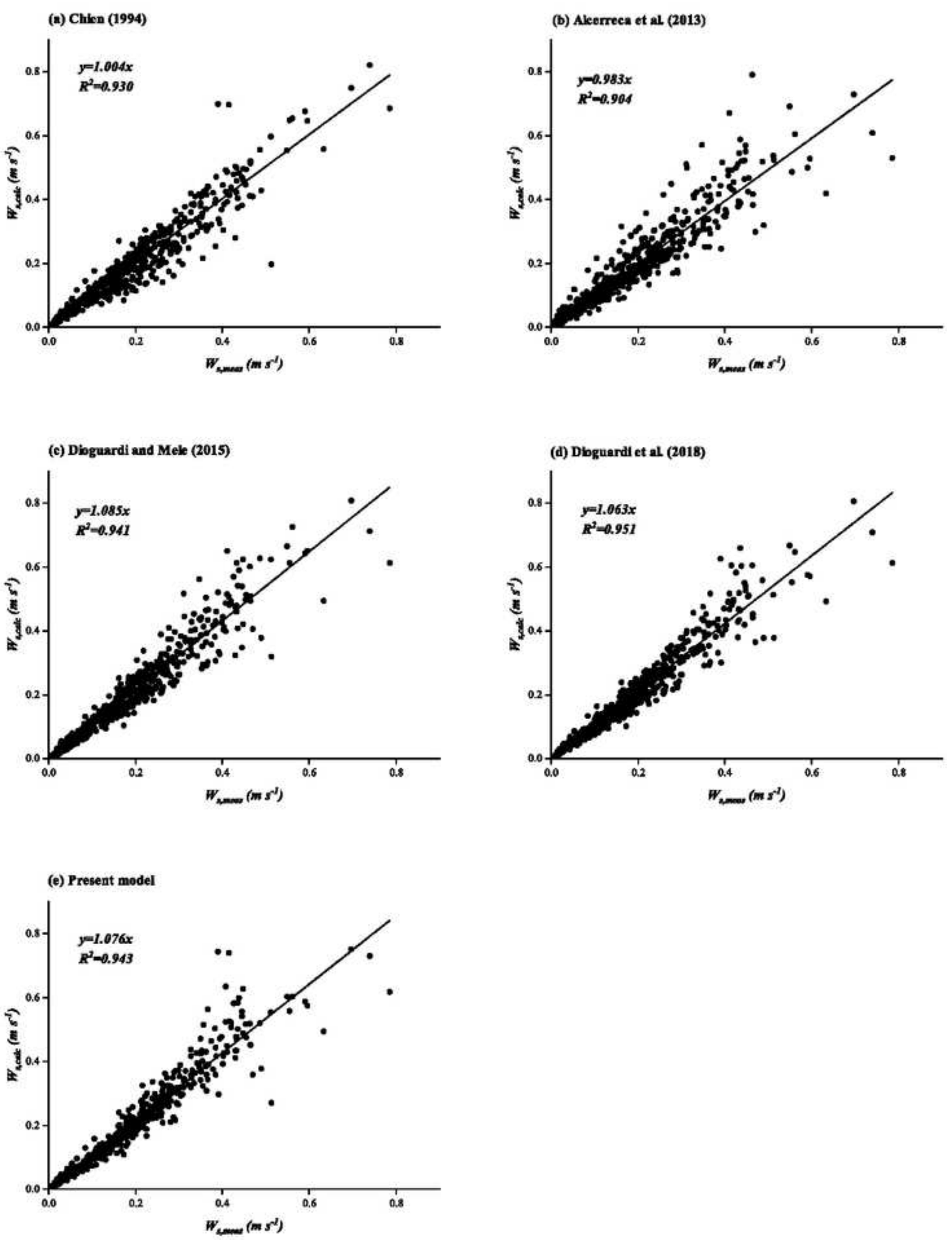

Figure 4

The comparison results are displayed, along with the correlation coefficient of each model.

Supplementary Files

This is a list of supplementary files associated with this preprint. Click to download.

- SupplementaryData.xlsx